Supplement of Biogeosciences, 18, 3147–3171, 2021
https://doi.org/10.5194/bg-18-3147-2021-supplement

Biogeosciences
Open Access

Supplement of

Simulating measurable ecosystem carbon and nitrogen dynamics with the mechanistically defined MEMS 2.0 model

Yao Zhang et al.

Correspondence to: Yao Zhang (yao.zhang@colostate.edu)

Table S1. Summary of the model structure comparison of the new generation process-based soil carbon models.

Model name	Note	Measureable pools	Simulate N	deep soil C	In vivo/ex vivo pathway	Explicit microbial pool	Rhizosphere and bulk soil	Validated with fractionation data	Reference
BAMS1		Chemical based	N	Y	N	Y	N	N	Riley et al. (2014)
BAMS2	Added nitrogen to BAMS1	Chemical based	Y	Y	N	Y	N	N	Tang et al. (2019)
COMISSION		Y	N	Y	Y	Y	N	Y; only one site	Ahrens et al. (2015)
CORPSE		Y	N	Y	N	Y	Y	Y; only two sites	Sulman et al. (2014)
FUN-CORPSE	CORPSE integrated with FUN model	Y	Y	Y	N	Y	Y	N	Sulman et al. (2017)
JSM (Jena Soil Model)	built upon COMISSION	Y	Y	Y	Y	Y	N	N	Yu et al. (2020)
MEMS V1		Y	N	N	Y	Y; only litter layer	N	Y	Robertson et al. (2019)
MEMS V2	Full ecosystem model of MEMS V1	Y	Y	Y	Y	Y	Y	Y	This study
MEND		Y	N	N	Y	Y	N	N	Wang et al. (2013)
MEND-CN	Added nitrogen to MEND	Y	Y	N	Y	Y	N	N	Wang et al. (2020)
Millennial		Y	N	N	N	Y	N	N	Abramoff et al. (2018)
MIMICS		Y	N	N	N	Y	N	N	Wieder et al. (2014)
MIMICS-CN	Added nitrogen to MIMIC	Y	Y	N	N	Y	N	N	Kyker-Snowman et al. (2020)
ORCHIDEE-SOM		N	N	Y	N	N	N	N	Tifafi et al. (2018)
ORCHIMIC		N	Y	N	N	N	N	N	(2018)
SOMic		Y	N	N	Y	Y	N	N	Woolf and Lehmann (2019)
T&C	SOC pools are similar to MEND	Y	Y	N	Y	Y	N	N	Fatichi et al. (2019)

Table S2. List of major equations in the model. Variable definitions can be found in Tab. S3.

Equations	**Number**
Surface litter	
$\frac{dC_{Ssoluble}}{dt} = -C_{Ssoluble} * k_{soluble} * T_{eff} * W_{eff} * LCI_{eff} * MicCN_{eff} - C_{Ssoluble} * k_{solubleLeach} * W_{leach} + C_{Shydro} * k_{hydro} * T_{eff} * W_{eff} * LCI_{eff} * MicCN_{eff} + C_{Sunhydro} * k_{unhydro} * T_{eff} * W_{eff} * MicCN_{eff} + C_{SmicLitter} * k_{micDeath} * frac_{toSoluble}$	S1
$\frac{dC_{Shydro}}{dt} = -C_{Shydro} * k_{hydro} * T_{eff} * W_{eff} * LCI_{eff} * MicCN_{eff} - C_{Shydro} * k_{fragment} * T_{eff} * W_{eff} + C_{SmicLitter} * k_{micDeath} * frac_{toHydro}$	S2
$\frac{dC_{Sunhydro}}{dt} = -C_{Sunhydro} * k_{unhydro} * T_{eff} * W_{eff} * MicCN_{eff} - C_{Sunhydro} * k_{fragment} * T_{eff} * W_{eff} + C_{SmicLitter} * k_{micDeath} * frac_{toUnhydro}$ Note: unlike the soluble and hydrolysable pools, no LCI_{eff} on unhydrolysable pool decay.	S3
$\frac{dC_{SmicLitter}}{dt} = -C_{SmicLitter} * k_{micDeath} + C_{Ssoluble} * k_{soluble} * T_{eff} * W_{eff} * LCI_{eff} * MicCN_{eff} * CUE_{Ssoluble}$	S4
$\frac{dC_{SCO_2}}{dt} = C_{Ssoluble} * k_{soluble} * T_{eff} * W_{eff} * LCI_{eff} * MicCN_{eff} * (1 - CUE_{Ssoluble})$	S5
Rhizosphere litter	
$\frac{dC_{Rsoluble}}{dt} = -C_{Rsoluble} * k_{solubleLeach} * LCI_{eff} + C_{Rhydro} * k_{hydro} * T_{eff} * W_{eff} * LCI_{eff} * MicCN_{eff} + C_{Runhydro} * k_{unhydro} * T_{eff} * W_{eff} * MicCN_{eff} + C_{RmicLitter} * k_{micDeath} * frac_{toSoluble}$	S6
$\frac{dC_{Rhydro}}{dt} = -C_{Rhydro} * k_{hydro} * T_{eff} * W_{eff} * LCI_{eff} * MicCN_{eff} - C_{Rhydro} * k_{fragment} * T_{eff} * W_{eff} + C_{RmicLitter} * k_{micDeath} * frac_{toHydro}$	S7
$\frac{dC_{Runhydro}}{dt} = -C_{Runhydro} * k_{unhydro} * T_{eff} * W_{eff} * MicCN_{eff} - C_{Runhydro} * k_{fragment} * T_{eff} * W_{eff} + C_{RmicLitter} * k_{micDeath} * frac_{toUnhydro}$	S8
$\frac{dC_{RDOM}}{dt} = -C_{RDOM} * k_{soluble} * T_{eff} * W_{eff} * MicCN_{eff} - C_{RDOM} * k_{RDOMLeach} * WFPS^3 + C_{Rsoluble} * k_{solubleLeach} * LCI_{eff} + C_{exudate} * k_{exudate}$ Note: the decay rate of surface soluble litter $k_{soluble}$ is also used for RDOM.	S9
$\frac{dC_{RmicLitter}}{dt} = -C_{RmicLitter} * k_{micDeath} + C_{RDOM} * k_{soluble} * T_{eff} * W_{eff} * MicCN_{eff} * CUE_{RDOM}$	S10
$\frac{dC_{RCO_2}}{dt} = C_{RDOM} * k_{soluble} * T_{eff} * W_{eff} * MicCN_{eff} * (1 - CUE_{RDOM})$	S11

Bulk soil	
$\frac{\partial C_{POM}}{\partial t} = -C_{POM} * k_{POM} * T_{eff} * W_{eff} * MicCN_{eff} + C_{Shydro} * k_{fragment} * T_{eff} * W_{eff} + C_{Sunhydro} * k_{fragment} * T_{eff} * W_{eff} + C_{Rhydro} * k_{fragment} * T_{eff} * W_{eff} + C_{Runhydro} * k_{fragment} * T_{eff} * W_{eff} + C_{micBulk} * k_{micDeath} * frac_{toPOM} + D_{bioturb} \frac{\partial^2 (C_{POM})}{\partial z^2}$ Note: fluxes from surface litter only goes to the POM pool of the first soil layer.	S12
$\frac{\partial C_{DOM}}{\partial t} = -C_{dom} * k_{DOM} * T_{eff} * W_{eff} * MicCN_{eff} - C_{DOM} * k_{adsorpSMAOM} * WFPS^2 * frac_{toSMAOM} - W_{flux} \frac{\partial C_{DOM}}{\partial z} - k_{adsorpEMAOM} * C_{DOM} * (Sat_{EMAOM} - C_{EMAOM}) + k_{desorpEMAOM} * C_{EMAOM} + C_{micBulk} * k_{micDeath} * (1 - frac_{toPOM}) * (1 - frac_{toSMAOM}) + C_{POM} * k_{POM} * T_{eff} * W_{eff} * MicCN_{eff} + C_{RDOM} * k_{RDOMLeach} * WFPS^3 + D_{diff} \frac{\partial^2 (C_{DOM})}{\partial z^2} + C_{Ssoluble} * k_{solubleLeach} * W_{leach}$ Note: fluxes from surface litter only goes to the DOM pool of the first soil layer.	S13
$\frac{dC_{micBulk}}{dt} = -C_{micBulk} * k_{micDeath} + C_{dom} * k_{dom} * T_{eff} * W_{eff} * MicCN_{eff} * CUE_{DOM} + C_{SMAOM} * k_{SMAOM} * T_{eff} * W_{eff} * MicCN_{eff} * CUE_{SAMOM}$	S14
$\frac{dC_{SMAOM}}{dt} = -C_{SMAOM} * k_{SMAOM} * T_{eff} * W_{eff} * MicCN_{eff} + C_{micBulk} * k_{micDeath} * (1 - frac_{toPOM}) * frac_{toSMAOM} + C_{DOM} * k_{adsorpSMAOM} * WFPS^2 * frac_{toSMAOM}$	S15
$\frac{dC_{BCO_2}}{dt} = C_{dom} * k_{DOM} * T_{eff} * W_{eff} * MicCN_{eff} * (1 - CUE_{DOM}) + C_{SMAOM} * k_{SMAOM} * T_{eff} * W_{eff} * MicCN_{eff} * (1 - CUE_{SAMOM})$	S16
$C_{EMAOM} = Sat_{EMAOM} * \frac{lk_{EMAOM} * C_{DOM}}{1 + lk_{EMAOM} * C_{DOM}}$ Note: the Langmuir isotherm was used. It assumes instantaneous equilibrium, resulting in $lk_{EMAOM} = \frac{k_{adsorpEMAOM}}{k_{desorpEMAOM}}$	S17
Other	
$CUE = micCN_{max}/(CN_{substrate} + CN_{CUE\_km})$ when $CUE \leq CUE_{max}$ $CUE = CUE_{max}$ when $CUE > CUE_{max}$	S18
$CN_{substrate} = C_{substrate}/(N_{substrate} + N_{mineral\_avail})$	S19
$frac_{toSMAOM} = (1 - \frac{Sand}{100}) * (1 - \frac{C_{SMAOM}}{Sat_{SMAOM}})$	S20
$lk_{EMAOM} = coeff_{lk} * 10^{-0.186*pH-0.216}$	S21
$LCI_{eff} = (LCI_{max} - LCI)/(LCI_{max} - LCI_{min})$ when $LCI \geq LCI_{min}$ $LCI_{eff} = 1$ when $LCI < LCI_{min}$ Note: if $LCI_{eff} < LCI_{eff\_min}$, then $LCI_{eff} = LCI_{eff\_min}$	S22

$N_{mineral\_demand} = C_{Ssoluble} * k_{soluble} * T_{eff} * W_{eff} * LCI_{eff} * MicCN_{eff} * CUE_{Ssoluble}/micCN_{min}$ Note: for other pools that used by microbes, similar equations were used.	S23
$Sat_{EMAOM} = (coeff_{sat1} * (1 - Sand) + coeff_{sat2}) * frac_{EMAOMSat}$	S24
$Sat_{SMAOM} = (coeff_{sat1} * (1 - Sand) + coeff_{sat2}) * (1 - frac_{EMAOMSat})$	S25
$T_{eff} = \frac{\frac{\pi}{2} + \mathrm{atan}\left(coeff_{t1} * (T - coeff_{t2})\right)}{\pi}$	S26
$W_{eff} = \frac{1}{1 + coeff_{w1} * e^{(-coeff_{w2} * W_{rel})}}$	S27
$W_{rel} = \frac{SWC - SWC_r}{SWC_{FC} - SWC_r}$ when $SWC < SWC_{FC}$ $W_{rel} = 1$ when $SWC \geq SWC_{FC}$	S28

Table S3. List of variables used in equations in Tab. S2.

Variable	Definition	Unit
$C_{Ssoluble}$	Carbon in the soluble pool of surface litter	g C m-2
C_{Shydro}	Carbon in the hydrolysable pool of surface litter	g C m-2
$C_{Sunhydro}$	Carbon in the unhydrolysable pool of surface litter	g C m-2
$C_{SmicLitter}$	Carbon of the microbial pool in the surface litter	g C m-2
C_{SCO_2}	Carbon of the respired CO_2 from the surface litter decomposition	g C m-2
$C_{Rsoluble}$	Carbon in the soluble pool of rhizosphere litter	g C m-2
C_{Rhydro}	Carbon in the hydrolysable pool of rhizosphere litter	g C m-2
$C_{Runhydro}$	Carbon in the unhydrolysable pool of rhizosphere litter	g C m-2
$C_{RmicLitter}$	Carbon of the microbial pool in the rhizosphere litter	g C m-2
C_{SCO_2}	Carbon of the respired CO_2 from the rhyzosphere litter decomposition	g C m-2
$C_{micBulk}$	Carbon of the microbial pool in the bulk soil	g C m-2
C_{RDOM}	Carbon in the rhizosphere DOM pool	g C m-2
C_{DOM}	Carbon in the bulk soil DOM pool	g C m-2
C_{POM}	Carbon in the bulk soil POM pool	g C m-2
C_{EMAOM}	Carbon in the bulk soil exchangeable MAOM pool	g C m-2
C_{SMAOM}	Carbon in the bulk soil stable MAOM pool	g C m-2
$C_{exudate}$	Carbon in the root exudate	g C m-2
C_{BCO_2}	Carbon of the respired CO_2 from the bulk soil decomposition	g C m-2
$C_{substrate}$	Carbon of the substrate for decomposition	g C m-2
$CN_{substrate}$	C/N ratio of the substrate for decomposition	-
CN_{CUE_km}	Coefficient used to calculate CUE as a function of substrate C/N ratio	-
CUE	Carbon use efficiency	-
CUE_{max}	Maximum CUE	-
$CUE_{Ssoluble}$	Carbon use efficiency of the surface soluble pool decomposition	-
CUE_{RDOM}	Carbon use efficiency of the rhizosphere DOM pool decomposition	-
CUE_{DOM}	Carbon use efficiency of the bulk soil DOM pool decomposition	-
CUE_{SMAOM}	Carbon use efficiency of the bulk soil stable MAOM pool decomposition	-
$coeff_{sat}$	Two coefficients used for the linear regression that estimates the maximum sorption capacity of soil	-
$coeff_{lk}$	Scaling coefficient used to estimate the binding affinity for the sorption of eMAOM pool	-
$coeff_t$	Two coefficients used to define the temperature effect curve	-
$coeff_w$	Two coefficients used to define the moisture effect curve	-
$D_{bioturb}$	Maximum conductivity used for estimating bioturbation	cm^2 day^{-1}
D_{diff}	Diffusivity of solute	cm^2 s^{-1}
$frac_{toSoluble}$	Fraction of the carbon flow goes to soluble pool	-
$frac_{toHydro}$	Fraction of the carbon flow goes to hydrolysable pool	-
$frac_{toUnhydro}$	Fraction of the carbon flow goes to unhydrolysable pool	-
$frac_{toPOM}$	Fraction of the carbon flow goes to POM	-
$frac_{toSMAOM}$	Fraction of the carbon flow goes to stable MAOM pool	-
$frac_{EMAOMSat}$	Fraction of the maximum sorption capacity of soil that is exchangeable MAOM	-
$k_{soluble}$	Maximum decay rate of soluble litter at optimal temperature and moisture	day^{-1}
k_{hydro}	Maximum decay rate of hydrolysable litter at optimal temperature and moisture	day^{-1}
$k_{unhydro}$	Maximum decay rate of unhydrolysable litter at optimal temperature and moisture	day^{-1}
$k_{micDeath}$	Microbial death rate	day^{-1}
k_{DOM}	Maximum decay rate of bulk soil DOM at optimal temperature and moisture	day^{-1}
k_{POM}	Maximum decay rate of POM at optimal temperature and moisture	day^{-1}
k_{SMAOM}	Maximum decay rate of stable MAOM at optimal temperature and moisture	day^{-1}

$k_{exudate}$	Rate of exudate produced by root	day^{-1}
$k_{fragment}$	Maximum fragmentation rate of the litter hydrolysable pool and unhydrolysable pool	day^{-1}
$k_{solubleLeach}$	Maximum rate of soluble litter leached to soil	day^{-1}
$k_{RDOMLeach}$	Maximum rate of rhizosphere DOM leached to bulk soil	day^{-1}
$k_{adsorpSMAOM}$	Maximum rate of DOM adsorption to stable MAOM	day^{-1}
$k_{adsorpEMAOM}$	Rate of DOM adsorption to exchangeable MAOM	day^{-1}
$k_{desorpEMAOM}$	Rate of DOM desorption from exchangeable MAOM	day^{-1}
LCI	Lignocellulose index	-
LCI_{eff}	Effect of litter LCI on the reaction rate	-
LCI_{eff_min}	Minimum effect on litter decompostion corresponding to LCI_{min}	-
LCI_{max}	Maximum LCI used in the calculation of LCI effect on litter decomposition	-
LCI_{min}	Minimum LCI used in the calculation of LCI effect on litter decomposition	-
lk_{EMAOM}	Binding affinity for the sorption of eMAOM pool	g C day^{-1}
$MicCN_{eff}$	Effect of microbial C/N ratio on the reaction rate	-
$micCN_{max}$	Maximum C/N ratio of microbe	-
$micCN_{min}$	Minimum C/N ratio of microbe	-
$N_{substrate}$	Nitrogen of the substrate for decomposition	g N m^{-2}
$N_{mineral\_avail}$	Available mineral N for microbial uptake	g N m^{-2}
$N_{mineral\_demand}$	Microbial demand for mineral N	g N m^{-2}
pH	Soil pH	-
$Sand$	Sand content of soil	%
Sat_{EMAOM}	Maximum sorption capacity of soil for the exchangeable MAOM	g C m^{-2}
Sat_{SMAOM}	Maximum sorption capacity of soil for the stable MAOM	g C m^{-2}
SWC	Soil water content	-
SWC_r	Residual soil water content	-
SWC_{FC}	Soil water content at field capacity	-
T_{eff}	Temperature effect	-
W_{eff}	Moisture effect	-
W_{flux}	Amount of water flows from one soil layer to an adjacent layer	cm
W_{leach}	Amount of water flows from litter layer to soil	cm
W_{rel}	Relative water content (relative to water holding capacity)	-
$WFPS$	Water filled pore space	-
z	Depth from soil surface	cm

Table S4. List of parameters used in the plant growth submodel.

Parameter Name	Definition	Unit
perennial_flag	If perennial crop, use 1. For annual crop, use 0.	-
frac_Soluble_Leaf	Fraction of leaf litter allocated to soluble pool	-
frac_Unhydrol_Leaf	Fraction of leaf litter allocated to unhydrolysable pool	-
frac_Soluble_Stem	Fraction of stem litter allocated to soluble pool	-
frac_Unhydrol_Stem	Fraction of stem litter allocated to unhydrolysable pool	-
frac_Soluble_CoarseRoot	Fraction of coarse root litter allocated to soluble pool	-
frac_Unhydrol_CoarseRoot	Fraction of coarse litter allocated to unhydrolysable pool	-
frac_Soluble_FineRoot	Fraction of fine root litter allocated to soluble pool	-
frac_Unhydrol_FineRoot	Fraction of fine root litter allocated to unhydrolysable pool	-
root_water_h1	Matric head above which no water uptake	cm
root_water_h2	Matric head above which water uptake increase from 0 at "root_water_h1" to maximum extraction rate	cm
root_water_h3a	Matric head below which water uptake starts to decrease when potential transpiration rate is very high (0.5 cm/day)	cm
root_water_h3b	Matric head below which water uptake starts to decrease when potential transpiration rate is very low (0.1 cm/day)	cm
root_water_h4	Matric head below which there is no water uptake	cm
bulkDensityLitter	Bulk density of litter	g cm^{-3}
litterBio_FullCover	Amount of litter biomass to fully cover the soil.	g m^{-2}
wcSaturationLitter	Water content of litter at saturation	-
wcFieldCapacityLitter	Water content of litter at field capacity	-
wcThresLitter	Water content of litter threshold below which evaporation rate cannot meet the potential rate	-
phenoTemperature_Base	Base temperature for phenology	℃
phenoTemperature_Optimum	Optimum temperature for phenology	℃
phenoTemperature_Ceiling	Ceiling temperature for phenology	℃
phenoTemperature_Curvature	Curvature for temperature response for phenology	-
photoPeriodType	Photo period type: 0 for crop type not sensitive to photoperiod, 1 for short-day, 2 for long-day	-
photoPeriod_Critical	Critical photoperiod	hour
photoperiod_Start	Phenology stage when photoperiod sensitive phase start	-
photoperiod_End	Phenology stage when photoperiod sensitive phase end	-
photoPeriodSensitivity	Photo period sensitivity	-
thurmalUnits_Vegetative	Minimum thermal units for vegetative phase	℃
thurmalUnit_Reproductive	Minimum thermal units for reproductive phase	℃
radiationUseEfficiency	Radiation use efficiency (RUE) for total biomass	g biomass MJ PAR^{-1}
RUETemperature_Base	Base temperature for RUE	℃
RUETemperature_OptLower	Lower temperature for optimal RUE	℃
RUETemperature_OptUpper	Upper temperature for optimal RUE	℃
RUETemperature_Ceiling	Ceiling temperature for RUE	℃

klight	Light extinction coefficient	-
transp_k_max	Crop coefficient for transpiration at full canopy cover	-
coeff_NitrogenStressRUE	Coefficient for nitrogen stress on RUE	-
specificLeafArea	Specific leaf area	m^2 leaf area g^{-1}
rootDepth_max	Maximum rooting depth	cm
rootDepth50	The depth from surface to which 50% of the root mass is distributed.	cm
totalBiomass_init	Initial total biomass at emergence	g m^{-2}
frac_ToBlg_init	Fraction of initial biomass that is in root	-
stage_RootFracDecrease	Phenology stage at which allocation fraction of NPP to root reduces	-
stage_RootFracZero	Phenology stage at which allocation fraction of NPP to root is 0	-
frac_BlgToFineRoot_End	Fraction of belowground NPP that is allocated to fine root at the end of root growth state	-
frac_BlgToExudate	Fraction of below ground NPP that is allocated to exudate	-
frac_AbgToLeaf_init	Fraction of aboveground NPP that is allocated to leaf at the beginning of growth	-
Stage_LeafFracDecrease	Phenology stage at which allocation of NPP to leaf is decreasing	-
Stage_LeafFracZero	Phenology stage at which allocation of NPP to leaf is 0	-
GreenLeafWeightRatio_LAImax	Green leaf weight ratio at maximum LAI	-
GreenLeafWeightRatio_PM	Green leaf weight ratio at physiological maturity	-
frac_AbgToStem_DS1	Fraction of aboveground NPP that is allocated to stem at the beginning of reproductive stage	-
Stage_StemFracZero	Phenology stage at which allocation of NPP to stem is 0	-
frac_C_VegOrgan	Carbon content of vegetative organs	g C g biomass^{-1}
efficiencyVegOrgan	Growth efficiency for vegetative organs	-
frac_C_Seed	Carbon content of seed	g C g biomass^{-1}
efficiencySeed	Growth efficiency for seed	-
LeafNitrogenConc_min	Minimum nitrogen content of leaf	g N g biomass^{-1}
StemNitrogenConc_min	Minimum nitrogen content of stem	g N g biomass^{-1}
RootNitrogenConc_min	Minimum nitrogen content of coarse and fine root	g N g biomass^{-1}
Exudate_NitrogenConc_min	Minimum nitrogen content of exudate	g N g biomass^{-1}
SeedNitrogenConc_max	Maximum nitrogen content of seed	g N g biomass^{-1}
LeafNitrogenConc_max_DS0	Maximum nitrogen content of leaf at the beginning of growth	g N g biomass^{-1}
LeafNitrogenConc_max_DS1	Maximum nitrogen content of leaf at the beginning of reproductive stage	g N g biomass^{-1}
StemNitrogenConc_max_fracLeaf	Maximum nitrogen content of stem as a fraction of leaf	g N g biomass^{-1}
CoarseRootNitrogenConc_max_fracLeaf	Maximum nitrogen content of coarse root as a fraction of leaf	g N g biomass^{-1}
FineRootNitrogenConc_max_fracLeaf	Maximum nitrogen content of fine root as a fraction of leaf	g N g biomass^{-1}

ExudateNitrogenConc_max_fracLeaf	Maximum nitrogen content of exudate as a fraction of leaf	g N g biomass^{-1}
Stage_CoarseRootDeath_start	Phenology stage at which coarse root start to die	-
frac_CoarseRootDeath	Death rate of coarse root	day^{-1}
frac_FineRootDeath	Death rate of fine root	day^{-1}
Stage_StemDeath_start	Phenology stage at which stem start to die	-
frac_StemDeath	Death rate of stem	day^{-1}
Stage_tanslocToSeed_start	Phenology stage at which translocation of nitrogen to seed starts	-
Coeff_transloc	Coefficient for nitrogen translocation to seed	day^{-1}
frac_stem_senscence	Rate of stem becomes senescence at the end of growing season for perennials	day^{-1}
frac_root_senescence	Rate of root becomes senescence at the end of growing season for perennials	day^{-1}
frac_stem_storage	Maximum fraction of stem is storage of carbohydrate that can be used for regrowth from defoliation and initial growth at the beginning of a growing season	day^{-1}
ratio_ShootRoot_crit	The critical shoot root ratio below which more photosynthate is allocated aboveground	-
frac_StandingDeadFall	Rate of standing dead biomass falls to become litter	day^{-1}

Table S5. Sources of the input data for model simulations of the NEON sites.

Input data	Source	Reference
Weather	High Plains Regional Climate Center database; SCAN database	https://hprcc.unl.edu/ (accessed on 02/13/2020); Schaefer et al. (2007)
Historical fire frequency	Historical fire frequency map	Guyette et al. (2012)
Recent fire frequency and time	NEON database	NEON (2020e)
Total atmospheric N deposition	Total atmospheric N deposition map	Hember (2018)
Biological N fixation	Regression on actual ET	Cleveland et al. (1999)
Actual ET for calculation of Biological N fixation	MODIS Land Subset Products	https://modis.ornl.gov/ (accessed on 05/12/2020); ORNL DAAC (2018); Running et al. (2017)
NPP	MODIS Land Subset Products	https://modis.ornl.gov/ (accessed on 05/12/2020); ORNL DAAC (2018); Running et al. (2015)
Water potentials for root water uptake	Field measurements	(2001)
C and N removed from fire	Field measurements	Ojima (1990)
Aboveground and belowground C allocation	Aboveground and belowground NPP maps	Bradford et al. (2005)
Soil physical property	NEON database	NEON (2020)
Soil chemical property	NEON database	NEON (2020b)
Plant aboveground physical and chemical properties	NEON database	NEON (2020c)
Root chemical properties	NEON database	NEON (2020d)

Table S6. Soil properties for the Soil Climate Analysis Network (SCAN) sites used for soil water and temperature validation.

	Bushland, TX	Fort Assiniboine, MT	Nunn, CO	Rogers Farm, NE
0 – 20 cm				
Sand (%)	21.2	33.4	70.6	6.5
Clay (%)	27.0	22.6	17.6	36.0
Bulk Density (g cm^{-3})	1.3	1.3	1.5	1.4
Organic C (%)	2.5	1.3	0.9	2.3
20 – 50 cm				
Sand (%)	15.5	27.8	73.3	4.3
Clay (%)	45.3	29.9	17.1	41.9
Bulk Density (g cm^{-3})	1.4	1.3	1.6	1.3
Organic C (%)	0.8	0.9	0.4	1.1
50 – 100 cm				
Sand (%)	14.8	36.0	73.4	4.2
Clay (%)	39.8	23.7	16.2	36.8
Bulk Density (g cm^{-3})	1.5	1.6	1.5	1.4
Organic C (%)	0.4	0.4	0.1	0.4

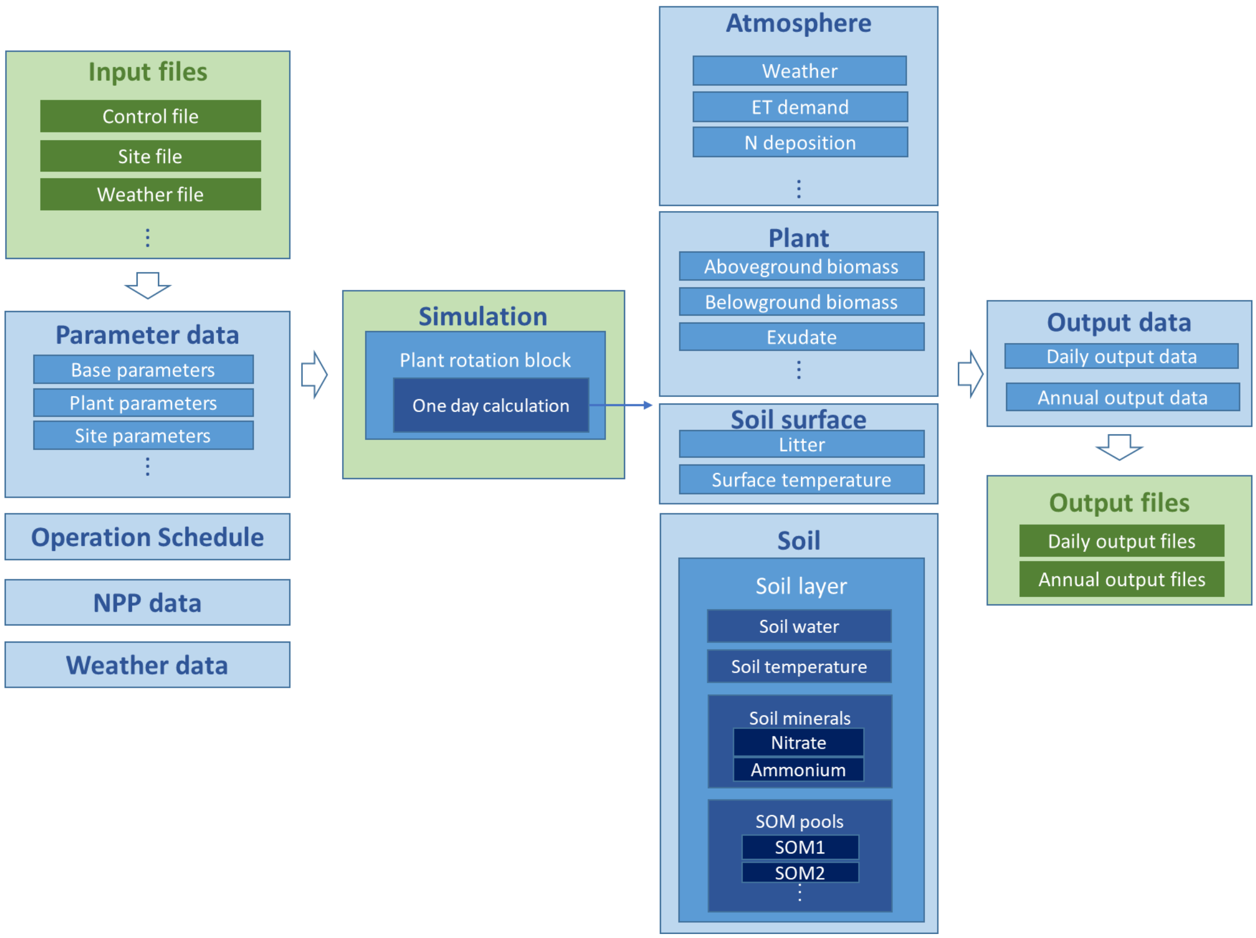

Figure S1. The structure of the model in Java. Each box represents one or a set of objects in Java.

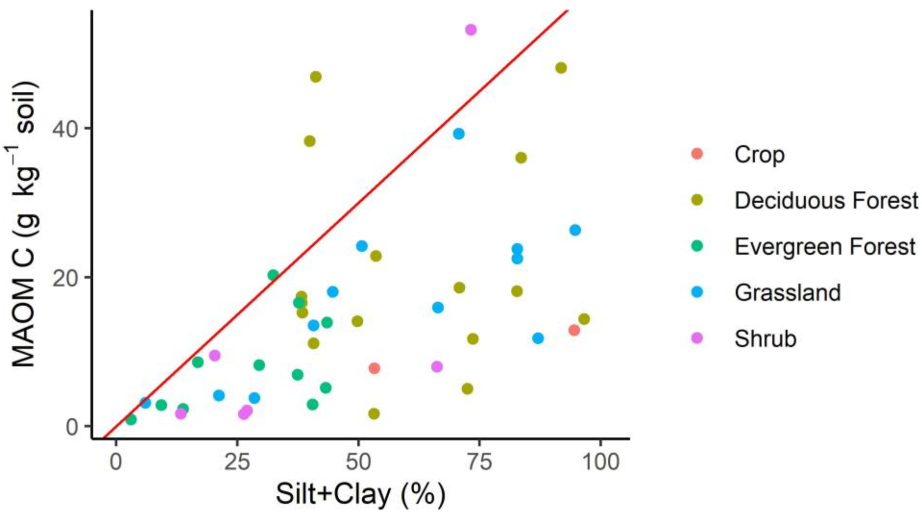

Figure S2. The fitted saturation curve using measured mineral-associated (MAOM) carbon from this study and soil texture data from the NEON database.

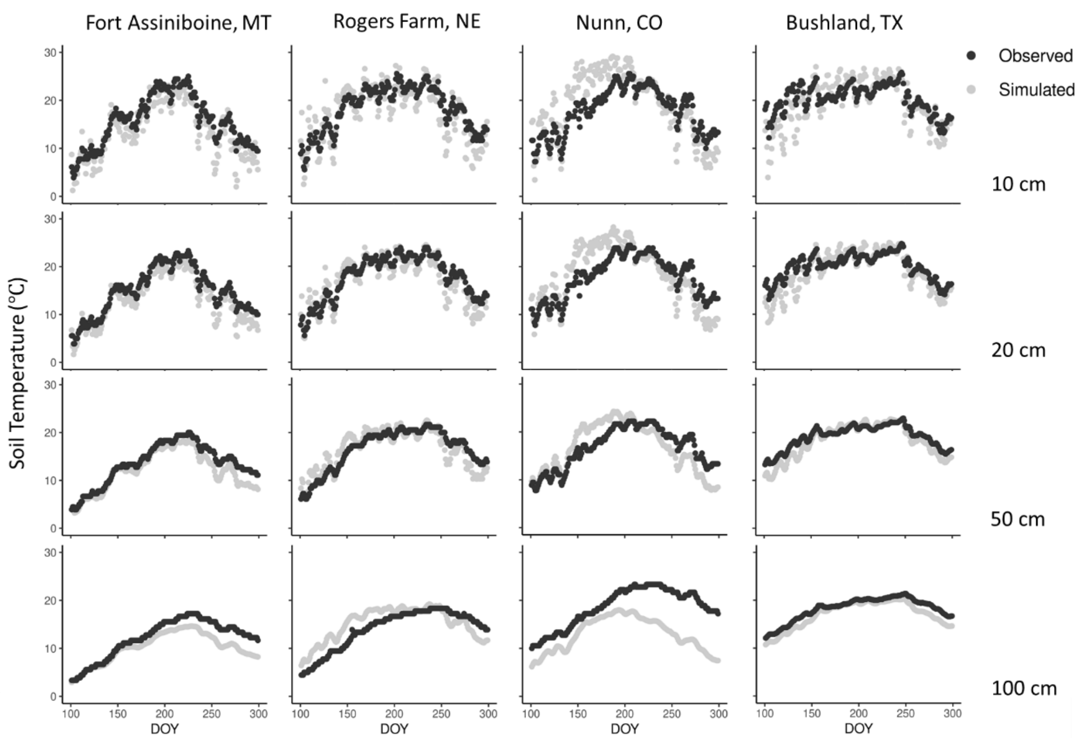

Figure S3. An example of simulated soil temperature in comparison with measurements of four Soil Climate Analysis Network (SCAN) sites. Daily average data in 2014 were presented. The statistics can be found in Table 4.

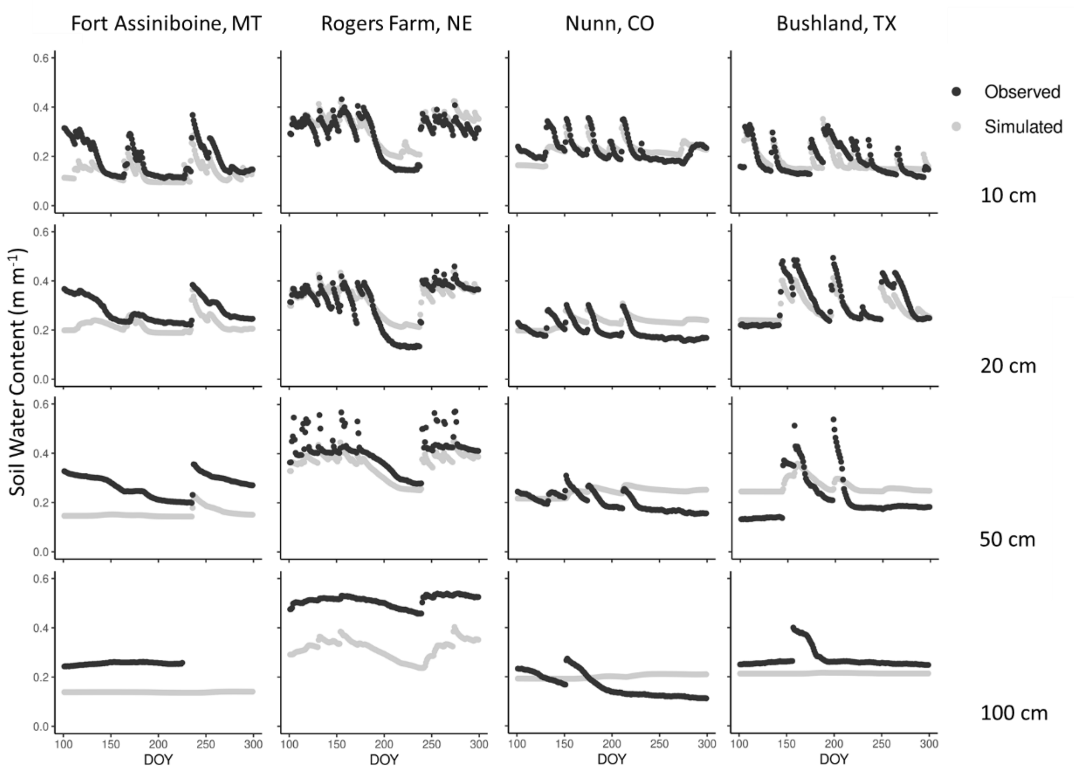

Figure S4. An example of simulated soil water content in comparison with measurements of four Soil Climate Analysis Network (SCAN) sites. Daily average data in 2014 were presented. The statistics can be found in Table 4.

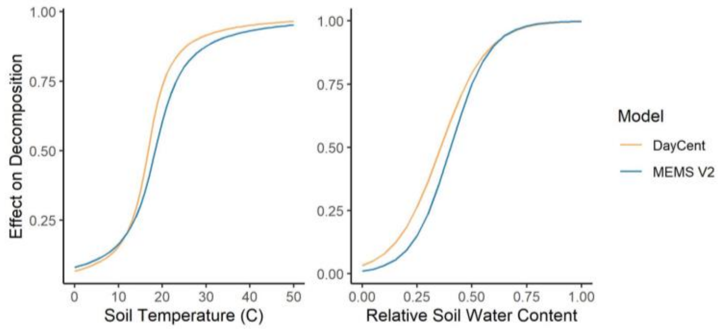

Figure S5. The calibrated curves for temperature and moisture effect on decomposition used in the MEMS 2.0 model. The curves are compared with those in the DayCent model.

References in the Supplementary Materials

Abramoff, R., Xu, X., Hartman, M., O'Brien, S., Feng, W., Davidson, E., Finzi, A., Moorhead, D., Schimel, J., Torn, M. and Mayes, M. A.: The Millennial model: in search of measurable pools and transformations for modeling soil carbon in the new century, Biogeochemistry, 137(1), 51–71, https://doi.org/10.1007/s10533-017-0409-7, 2018.

Ahrens, B., Braakhekke, M. C., Guggenberger, G., Schrumpf, M. and Reichstein, M.: Contribution of sorption, DOC transport and microbial interactions to the 14C age of a soil organic carbon profile: Insights from a calibrated process model, Soil Biology and Biochemistry, 88, 390–402, https://doi.org/10.1016/j.soilbio.2015.06.008, 2015.

Bradford, J. B., Lauenroth, W. K. and Burke, I. C.: The Impact of Cropping on Primary Production in the U.s. Great Plains, Ecology, 86(7), 1863–1872, https://doi.org/10.1890/04-0493, 2005.

Cleveland, C. C., Townsend, A. R., Schimel, D. S., Fisher, H., Howarth, R. W., Hedin, L. O., Perakis, S. S., Latty, E. F., Fischer, J. C. V., Elseroad, A. and Wasson, M. F.: Global patterns of terrestrial biological nitrogen (N2) fixation in natural ecosystems, Global Biogeochemical Cycles, 13(2), 623–645, https://doi.org/10.1029/1999GB900014, 1999.

Davidson, E. A., Samanta, S., Caramori, S. S. and Savage, K.: The Dual Arrhenius and Michaelis–Menten kinetics model for decomposition of soil organic matter at hourly to seasonal time scales, Global Change Biology, 18(1), 371–384, https://doi.org/10.1111/j.1365-2486.2011.02546.x, 2012.

De Jong, R. and MacDonald, K. B.: Water balance components in the Canadian mixed wood ecozone, in Sustaining the Global Farm, 10th International Soil, , 2001.

Fatichi, S., Manzoni, S., Or, D. and Paschalis, A.: A Mechanistic Model of Microbially Mediated Soil Biogeochemical Processes: A Reality Check, Global Biogeochemical Cycles, 33(6), 620–648, https://doi.org/10.1029/2018GB006077, 2019.

Guyette, R. P., Stambaugh, M. C., Dey, D. C. and Muzika, R.-M.: Predicting Fire Frequency with Chemistry and Climate, Ecosystems, 15(2), 322–335, https://doi.org/10.1007/s10021-011-9512-0, 2012.

Hember, R. A.: Spatially and temporally continuous estimates of annual total nitrogen deposition over North America, 1860–2013, Data in Brief, 17, 134–140, https://doi.org/10.1016/j.dib.2017.12.052, 2018.

Huang, Y., Guenet, B., Ciais, P., Janssens, I. A., Soong, J. L., Wang, Y., Goll, D., Blagodatskaya, E. and Huang, Y.: ORCHIMIC (v1.0), a microbe-mediated model for soil organic matter decomposition, Geoscientific Model Development, 11(6), 2111–2138, https://doi.org/10.5194/gmd-11-2111-2018, 2018.

Kyker-Snowman, E., Wieder, W. R., Frey, S. D. and Grandy, A. S.: Stoichiometrically coupled carbon and nitrogen cycling in the MIcrobial-MIneral Carbon Stabilization model version 1.0 (MIMICS-CN v1.0), Geoscientific Model Development, 13(9), 4413–4434, https://doi.org/10.5194/gmd-13-4413-2020, 2020.

NEON: Data Product DP1.00096.001, Soil physical properties (Megapit), National Ecological Observatory Network, Battelle, Boulder, CO, USA. http://data.neonscience.org, last access: 12 May 2020a, 2020.

NEON: Data Product DP1.10008.001, Soil chemical properties (Distributed initial characterization)., National Ecological Observatory Network, Battelle, Boulder, CO, USA. http://data.neonscience.org, last access: 12 May 2020b, 2020.

NEON: Data Product DP1.10026.001, Plant foliar physical and chemical properties, National Ecological Observatory Network, Battelle, Boulder, CO, USA. http://data.neonscience.org, last access: 12 May 2020c, 2020.

NEON: Data Product DP1.10102.001, Root chemical properties, National Ecological Observatory Network, Battelle, Boulder, CO, USA. http://data.neonscience.org, last access: 12 May 2020d, 2020.

NEON: Data Product DP1.10111.001, Site management and event reporting, National Ecological Observatory Network, Battelle, Boulder, CO, USA. http://data.neonscience.org, last access: 12 May 2020e, 2020.

Ojima, D. S.: Simulated impacts of annual burning on prairie ecosystems, in Fire in North American Prairies, Norman, University of Oklahoma Press, , 1990.

ORNL DAAC: MODIS and VIIRS Land Products Global Subsetting and Visualization Tool. ORNL DAAC, Oak Ridge, Tennessee, USA. https://doi.org/10.3334/ORNLDAAC/1379, 2018.

Riley, W. J., Maggi, F., Kleber, M., Torn, M. S., Tang, J. Y., Dwivedi, D. and Guerry, N.: Long residence times of rapidly decomposable soil organic matter: application of a multi-phase, multi-component, and vertically resolved model (BAMS1) to soil carbon dynamics, Geoscientific Model Development, 7(4), 1335–1355, https://doi.org/10.5194/gmd-7-1335-2014, 2014.

Robertson, A. D., Paustian, K., Ogle, S., Wallenstein, M. D., Lugato, E. and Cotrufo, M. F.: Unifying soil organic matter formation and persistence frameworks: the MEMS model, Biogeosciences, 16(6), 1225–1248, https://doi.org/10.5194/bg-16-1225-2019, 2019.

Running, S., Mu, Q. and Zhao, M.: MOD17A3H MODIS/Terra Net Primary Production Yearly L4 Global 500m SIN Grid V006. NASA EOSDIS Land Processes DAAC, https://doi.org/10.5067/MODIS/MOD17A3H.006, 2015.

Running, S., Mu, Q. and Zhao, M.: MOD16A2 MODIS/Terra Net Evapotranspiration 8-Day L4 Global 500m SIN Grid V006. NASA EOSDIS Land Processes DAAC, https://doi.org/10.5067/MODIS/MOD16A2.006, 2017.

Schaefer, G. L., Cosh, M. H. and Jackson, T. J.: The USDA Natural Resources Conservation Service Soil Climate Analysis Network (SCAN), J. Atmos. Oceanic Technol., 24(12), 2073–2077, https://doi.org/10.1175/2007JTECHA930.1, 2007.

Sihi, D., Davidson, E. A., Chen, M., Savage, K. E., Richardson, A. D., Keenan, T. F. and Hollinger, D. Y.: Merging a mechanistic enzymatic model of soil heterotrophic respiration into an ecosystem model in two AmeriFlux sites of northeastern USA, Agricultural and Forest Meteorology, 252, 155–166, https://doi.org/10.1016/j.agrformet.2018.01.026, 2018.

Sulman, B. N., Phillips, R. P., Oishi, A. C., Shevliakova, E. and Pacala, S. W.: Microbe-driven turnover offsets mineral-mediated storage of soil carbon under elevated CO 2, Nature Climate Change, 4(12), 1099–1102, https://doi.org/10.1038/nclimate2436, 2014.

Sulman, B. N., Brzostek, E. R., Medici, C., Shevliakova, E., Menge, D. N. L. and Phillips, R. P.: Feedbacks between plant N demand and rhizosphere priming depend on type of mycorrhizal association, Ecology Letters, 20(8), 1043–1053, https://doi.org/10.1111/ele.12802, 2017.

Tang, F. H. M., Riley, W. J. and Maggi, F.: Hourly and daily rainfall intensification causes opposing effects on C and N emissions, storage, and leaching in dry and wet grasslands, Biogeochemistry, 144(2), 197–214, https://doi.org/10.1007/s10533-019-00580-7, 2019.

Tifafi, M., Camino-Serrano, M., Hatté, C., Morras, H., Moretti, L., Barbaro, S., Cornu, S. S. and Guenet, B.: The use of radiocarbon ^{14}C to constrain carbon dynamics in the soil module of the land surface model ORCHIDEE (SVN r5165), Geoscientific Model Development Discussions, 1–24, https://doi.org/10.5194/gmd-2018-102, 2018.

Wang, G., Post, W. M. and Mayes, M. A.: Development of microbial-enzyme-mediated decomposition model parameters through steady-state and dynamic analyses, Ecological Applications, 23(1), 255–272, https://doi.org/10.1890/12-0681.1, 2013.

Wang, G., Huang, W., Zhou, G., Mayes, M. A. and Zhou, J.: Modeling the processes of soil moisture in regulating microbial and carbon-nitrogen cycling, Journal of Hydrology, 585, 124777, https://doi.org/10.1016/j.jhydrol.2020.124777, 2020.

Wieder, W. R., Grandy, A. S., Kallenbach, C. M. and Bonan, G. B.: Integrating microbial physiology and physio-chemical principles in soils with the MIcrobial-MIneral Carbon Stabilization (MIMICS) model, Biogeosciences, 11(14), 3899–3917, https://doi.org/10.5194/bg-11-3899-2014, 2014.

Woolf, D. and Lehmann, J.: Microbial models with minimal mineral protection can explain long-term soil organic carbon persistence, Scientific Reports, 9(1), 6522, https://doi.org/10.1038/s41598-019-43026-8, 2019.

Yu, L., Ahrens, B., Wutzler, T., Schrumpf, M. and Zaehle, S.: Jena Soil Model (JSM v1.0; revision 1934): a microbial soil organic carbon model integrated with nitrogen and phosphorus processes, Geoscientific Model Development, 13(2), 783–803, https://doi.org/10.5194/gmd-13-783-2020, 2020.